

# TiO<sub>2</sub> / ZnO Photocatalytic Activity for Hydrogen Production

Meshal S.Al-Johani<sup>1</sup>, Yousef S.Al-Zaghayer<sup>2a</sup>, Sulaiman I.Al-Mayman<sup>1</sup>

<sup>1</sup>Water and Energy Research Institute (WERI), King Abdulaziz City for Science and Technology, P.O.Box 6086 Riyadh 11442 Saudi Arabia  
Maljuhni@kacst.edu.sa

<sup>2</sup>Department of Chemical Engineering, King Saud University (KSU)  
P.O. Box 800, Riyadh 11421, Saudi Arabia  
<sup>a</sup>Director of Industrial Catalysts Chair

**Abstract**— The present work investigates Zn doped TiO<sub>2</sub> (1.0, 5.0, 10.0, 12.0 and 30.0 wt.% Zn) photocatalysts were prepared by low cost sol-gel auto-ignition method and systematically investigate their structural, optical and surface morphological properties with X-ray diffractometer, UV-Vis spectrophotometer, Fourier Transform Infrared spectrometer (FTIR) and Scanning electron microscopy (SEM) with energy dispersive X-ray spectroscopy (EDX). The photocatalytic H<sub>2</sub> evolution of the TiO<sub>2</sub>-ZnO suspensions was evaluated in an aqueous ethanol medium (50 vol. %) under UV illumination. The Zn<sup>+2</sup> concentrations utilize to prepare TiO<sub>2</sub>-ZnO nanocomposites were found to have significant effect on the specific surface area, and photocatalytic activity. The H<sub>2</sub> evolution results obtained with TiO<sub>2</sub>-ZnO nanocomposites were compared with H<sub>2</sub> generation using commercial TiO<sub>2</sub> P25 and individual TiO<sub>2</sub> nanoparticles. The photocatalytic activity of TiO<sub>2</sub>-ZnO composite enhanced significantly as compared to bare TiO<sub>2</sub> nanoparticles and commercial TiO<sub>2</sub> P25. With respect to an increment in Zn<sup>+2</sup> doped, the photocatalytic activity of the composite increased and reaching an optimal H<sub>2</sub> production of 1048 μmol.h<sup>-1</sup> of catalyst for the TiO<sub>2</sub>-ZnO composite containing 10 wt.% Zn. These catalyst were proved in the photocatalytic water splitting and resulted seven times more active (1048 μmol.h<sup>-1</sup>) than the reference TiO<sub>2</sub> (150 μmol.h<sup>-1</sup>) and two times more active than TiO<sub>2</sub> P25 (595 μmol.h<sup>-1</sup>) semiconductors.

**Keywords**— Hydrogen production, Photocatalysts TiO<sub>2</sub>-ZnO, Photoconductors TiO<sub>2</sub>-ZnO, Water splitting.

## I. Introduction

In the past four decades the world population has doubled, which led to increased consumption of energy. The life style for people depends on energy which comes from oil, natural gas, methane and coal; therefore, renewable energy, such as solar, biofuel and nuclear should be utilized to resolve the issue of future energy demand because petroleum and all fossil fuels will be exhausted at some point [1]. When considering fuel sources, hydrogen is considered to be a promising carrier of solar-derived energy, and the use of hydrogen as an energy carrier has become so widespread that the term “hydrogen economy” has been coined [2-3]. Titanium dioxide is considered a promising photocatalyst for dye degradation [4-9], pesticides [10-12], atmospheric pollutants degradation [13] as well as for the inorganic pollutants removal from wastewater [14-15]. However, its use as a photocatalysts for

water splitting is limited due to its redox potential referring to the normal hydrogen electrode (NHE). A lot of studies have been made to increase the photocatalytic activity of titanium dioxide for the water splitting reaction. For this purpose, doped, mixed and co-catalysts with Fe, Zn, Cu, Ni, V, Mg, Be and Ni [16-17] and Pt, Pd, Ir, Rh, Ru [18] respectively were prepared to enhance the efficiency of hydrogen production. Recently, extraordinary attention has been focused on the synthesis of titania mixed oxides like CuO, ZnO, NiO and CeO [19–22] because these materials show important photocatalytic properties as well as potential applications in the water splitting. Here in this present work, ZnO has been chosen because it has the same band gap as TiO<sub>2</sub> and a slightly negative conduction band potential and, in principle, will have higher redox potential generating higher voltages [23-24]. Moreover, ZnO has direct band gap semiconductor with high exciton, binding energy and electron mobility than TiO<sub>2</sub> [25]. Up to now, ZnO based photocatalysts are limited due to photocorrosion upon irradiation but on the other hand, the efficiency of TiO<sub>2</sub> in solar processes are limited due to wide band gap and charge carrier recombination [26-27]. The main aim of the present work is to synthesize Zn doped TiO<sub>2</sub> photocatalysts using low cost sol-gel auto-ignition method and systematically investigate their structural, optical and surface morphological properties with x-ray diffractometer, UV-vis spectrophotometer, Fourier Transform Infrared spectrometer (FTIR) and scanning electron microscopy (SEM) with energy dispersive x-ray spectroscopy (EDX). In addition, the photocatalytic performance towards hydrogen generation is studied under Photochemical reactor connected with the gas chromatography.

## II. Experimental

### A. Catalyst Preparation

The nanostructured TiO<sub>2</sub>-ZnO samples were prepared by the sol-gel method. Samples of Zn doped TiO<sub>2</sub> with nominal compositions Ti<sub>1-x</sub>Zn<sub>x</sub>O<sub>2</sub> (x=0.0, 1.0, 5.0, 10.0, 12.0, and 30.0 %) have been prepared by sol-gel self-ignition method. Analytical grade of zinc nitrate [Zn(NO<sub>3</sub>)<sub>2</sub>·6H<sub>2</sub>O], titanium(IV) butoxide and citric acid [C<sub>6</sub>H<sub>8</sub>O<sub>7</sub>] were used as starting materials to prepare the nominal compositions. For this purpose, all materials according to their stoichiometric ratios were dissolved in de-ionized water. Citric acid was used

as catalyst to ignite the materials. Solution was heated at 100 °C on a hot plate with continuous magnetic stirring. As water evaporated, the solution became viscous and finally formed a highly viscous gel. Increasing the temperature up to about 300 °C led to the ignition of the gel. The dried gel burnt in a self-propagating combustion reaction until all the gel was completely burnt out to form a voluminous and fluffy powder with large surface area. Experimentally, it was observed that all the samples showed combustion behavior and burnt out completely to form a loose powder then the solid was ground to a fine powder in an agate mortar. Finally the as-burnt powders were annealed at 500 °C during 5 h in a static air atmosphere using a heating rate of 1 °C/min to convert them into anatase phase; finally the product was ground again. As reference pure TiO<sub>2</sub> sample was prepared in the same way described above but without Zn precursor.

### B. Catalyst characterization

In order to elucidate the difference in catalytic activities of catalyst, the prepared samples were characterized by various characterization techniques. The detail of these techniques is discussed below:

The crystalline structure of prepared samples were characterized with powder X-ray diffraction (XRD) on a Bruker D8 Discover X-ray diffractometer equipped with Cu K $\alpha$  radiation source operated at 40 Kv and 40 Ma. The diffraction intensity as a function of diffraction angle (2 $\theta$ ) was measured between 10-80°, using a step 0.03° and a counting time of 0.3 s per step. The specific surface area, pore volume and average pore diameter of the catalyst was measured in Micromeritics Tristar II 3020. Surface area and porosity analyzer by N<sub>2</sub> adsorption data at 77 K (-196 °C) according to the standard Brunauer Emmett Teller (BET) procedure. For each analysis 0.3 g of catalyst was used. Degassing of the samples was done at 250 °C for 3 h to remove the moisture content and other adsorbed gases from the surface of catalyst. The pore size distribution was calculated from desorption branch of the corresponding nitrogen isotherm by applying the Barrett, Joyner, and Halenda (BJH) method. Morphology of the prepared catalyst was observed using JEOL Scanning Electron Microscope system JEM-7600F. Elemental and chemical analysis of a sample obtained by EDS Analysis. Infrared spectrum of photocatalyst absorption was obtained by spectrum 100, Perkin Elmer Instruments. Perkin Elmer LAMBDA 35 UV-Visible diffuse reflectance spectroscopy was used to estimate band gap energy.

### C. Photocatalytic H<sub>2</sub> production

The photocatalytic hydrogen evolution over bare TiO<sub>2</sub>, commercial TiO<sub>2</sub>-P25 nanoparticles and coupled TiO<sub>2</sub>-ZnO nanocomposites was investigated in an aqueous media in the presence of ethanol as an electron donor under UV-light irradiation. The presence of an electron donor other than water is crucial for photocatalytic H<sub>2</sub> production. In this set-up, ethanol functions primarily as hole traps to prevent the rapid electron-hole recombination. The set-up consists of 1100 ml quartz semi-batch reactor provided with inner chamber placed inside the reactor for the lamp and jacket around the lamp for controlling temperature of the lamp. The reactor is a 7874.38

quartz Immersion Well, provided by Ace Glass Incorporated ACE. The irradiation was made using a high pressure Hg pen-lamp (with radiation of 254 nm and intensity of 2.2 mW/cm<sup>2</sup>) encapsulated in a quartz tube and immersed in the water solution. This lamp has part number 90-0012-01 provided by Ultra-Violet Products Ltd (UVP).

In a typical experiment, 0.8 g of TiO<sub>2</sub>- ZnO photocatalyst was dispersed in 400 ml water and 400 ml ethanol (50 vol. %) and placed in a quartz reactor. Prior to irradiation, the suspension of the catalyst was degassed with ultrapure nitrogen (N<sub>2</sub>) for 30 minute to completely remove the dissolved oxygen. The amount of hydrogen produced was followed by gas chromatography using a gas chromatograph (Trace GC Ultra) from Thermo Scientific equipped with a thermal conductivity detector and with a 5A column molecular sieve.

## III. Results and Discussions

### A. X-ray diffraction analysis (XRD)

The diffraction intensity as a function of the diffraction angle (2- $\theta$  degrees) was measured between 10° to 80° using a step width of 0.03°. Figure 1 shows the x-ray diffraction patterns of the Zn (0, 1, 5, 10, 12 and 30%) doped TiO<sub>2</sub> calcined at 500°C temperature. The powder XRD patterns show anatase titania phase formed which is confirmed by the peaks at (101) at 2 $\theta$ = 25.4° and (200) at 2 $\theta$ = 48.0° [28].

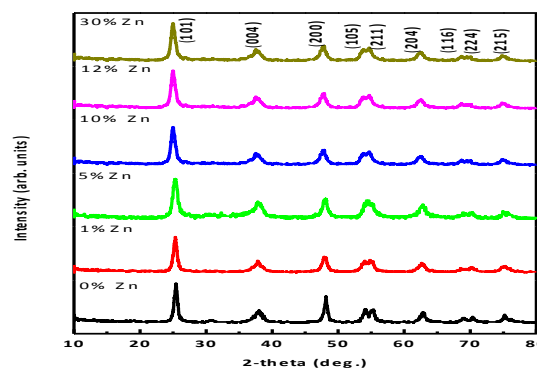


Fig. 1. X-ray diffraction patterns of the Zn (0, 1, 5, 10, 12 and 30

%) doped TiO<sub>2</sub> XRD profiles of TiO<sub>2</sub>- ZnO composites prepared with different Zn<sup>2+</sup> loading and calcined at 500 °C for 5 h.

It is noted that at highest Zn content (30 wt %), no diffraction peak of hexagonal ZnO appeared which is in line with studies of [29]. The XRD data of all the samples were Rietveld refined with HighScore Plus software version 3.0 e using a pseudo-Voigt profile function [30]. Figures 2,3 and 4 shows the Rietveld refined patterns of Zn (1, 5, 10, 12 and 30 %) doped TiO<sub>2</sub>.

It is clearly evident from the Rietveld-refinement that all the samples exhibit single-phase hexagonal structure. The Rietveld refinement factors of all the compositions are summarized in the Table I. Table I is showing the structural parameters lattice constant, R (expected, profile and weighted profile) with goodness of fit (GOF) which are extracted from Rietveld refinement. It is clear that there is a decrease in lattice parameters along c-axis due to the small ionic radius of zinc as compared to titanium [31].

Table I. Rietveld refined parameters.

Compositions	$R_{exp}$ (%)	$R_p$ (%)	$R_{wp}$ (%)	GOF	a (Å)	b (Å)	c (Å)
1% Zn	2.752	2.294	3.960	2.069	3.794	3.794	9.517
5 % Zn	2.930	2.758	4.470	2.327	3.794	3.794	9.499
10 % Zn	2.950	2.739	4.235	2.060	3.795	3.795	9.495
12 % Zn	10.550	9.934	17.450	2.731	3.783	3.783	9.472
30 % Zn	9.439	6.347	10.635	1.269	3.782	3.782	9.471

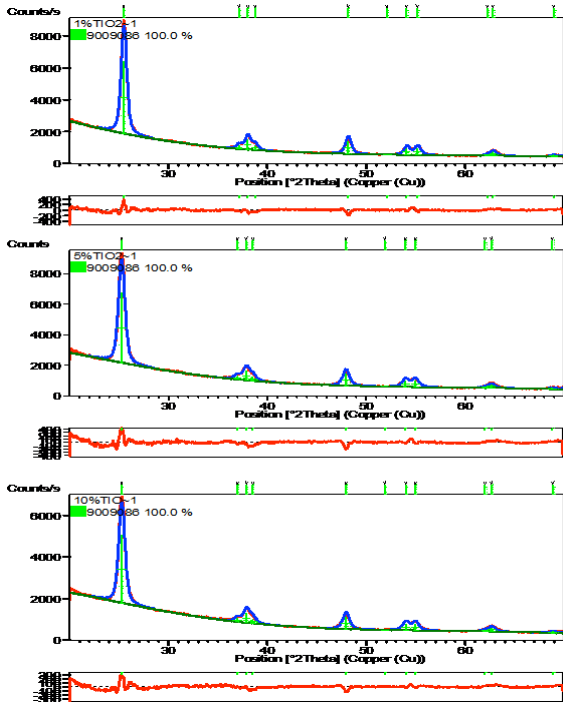


Fig. 2. Rietveld refinement of Zn (1, 5 and 10 %) doped TiO<sub>2</sub>

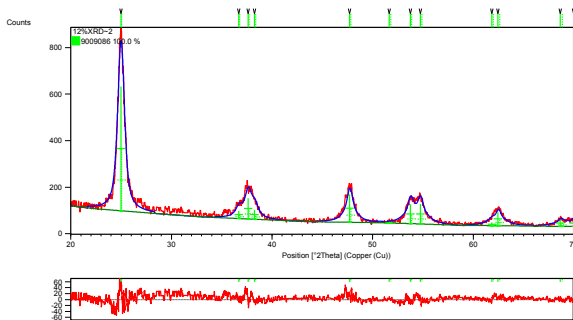


Fig. 3. Rietveld refinement of Zn 12% doped TiO<sub>2</sub>

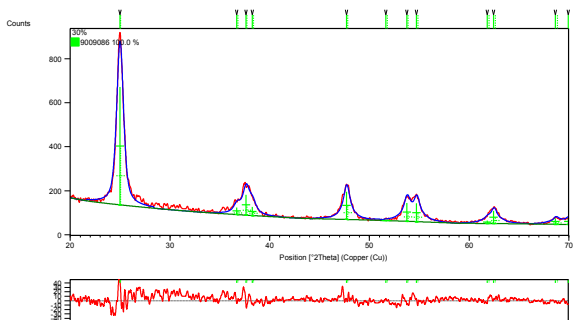


Fig. 4. Rietveld refinement of Zn 30% doped TiO<sub>2</sub>

#### B. Surface area and porosity analysis

The pore volume and pore size are calculated from desorption branch of the corresponding nitrogen isotherm by applying the Barrett, Joyner, and Halenda (BJH) method. Effects of ZnO loading on the BET specific surface areas, pore volumes (P.V), and pore diameters (P.D) are listed in Table II.

Table II. Textural properties of nanocomposite of TiO<sub>2</sub>-ZnO

ZnO(wt.%)	S <sub>BET</sub> (m <sup>2</sup> /g)	P.V (cm <sup>3</sup> /g)	P.D (nm)
TiO <sub>2</sub>	32.53	0.091	10.67
P25	46	0.09	30
1% Zn	52.08	0.085	5.81
5% Zn	63.44	0.093	5.19
10% Zn	69.93	0.1	5.04
12% Zn	64.01	0.1	5.93
30% Zn	36.64	0.062	6.19

Both the surface areas and pore volumes increased systematically with ZnO contents. Similar trends were observed after loading or mixing TiO<sub>2</sub> with ZnO or ZrO<sub>2</sub> [32,33]. The surface area and pore volume of TiO<sub>2</sub>-ZnO composite reached maximum with the 10 wt.% ZnO loadings. It was also found that the specific surface areas obtained from 1.0%, 5.0%, 10.0%, 12.0% and 30.0% wt.% Zn loadings were significantly higher than pure TiO<sub>2</sub>. Generally, higher surface area material is favorable for superior photocatalytic activity [34].

C. Scanning electron microscopy (SEM)/ Energy dispersive x-ray spectroscopy (EDX) investigations

Topography of the doped samples is found using Scanning Electron Microscope (SEM) JEOL Scanning Electron Microscope JEM-7600F. Figure 5 shows the SEM micrographs of Zn (0, 1, 5, 10, 12 and 30 %) doped TiO<sub>2</sub>. SEM micrographs for (B, C, D, E and F) confirm that Zn is uniformly distributed in TiO<sub>2</sub> without disturbing the anatase phase of TiO<sub>2</sub> as is also clear in the XRD patterns.

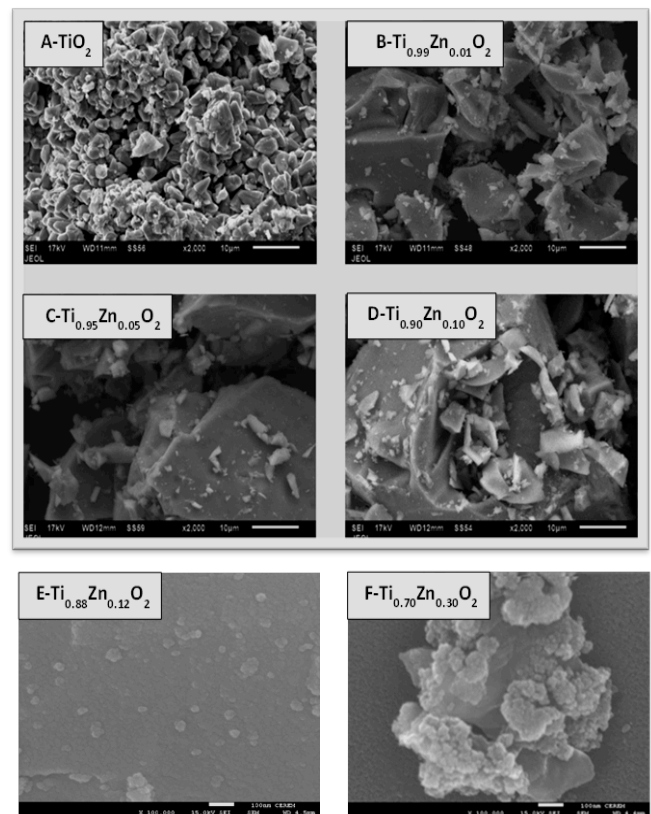


Fig. 5. SEM micrographs of Zn (0, 1, 5, 10, 12 and 30 %) doped TiO<sub>2</sub>.

Energy dispersive X-ray spectrometry (EDX) analysis of all the samples shows peaks of titanium, oxygen and zinc. There is no trace of any other impurities found within the detection limit of the EDX as shown in the Figure 6.

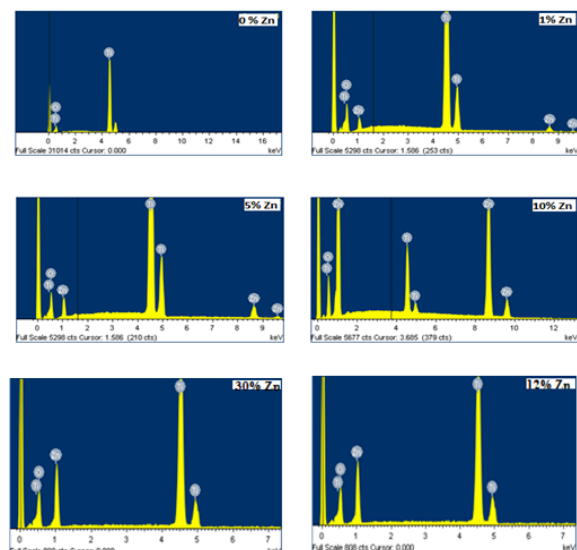


Fig. 6. EDX analysis of Zn (0, 1, 5, 10, 12 and 30 %) doped TiO<sub>2</sub>.

The quantitative elemental analysis of all the samples are assembled in Table III.

Table III. Quantitative EDX analysis of Zn (0, 1, 5,10, 12, and 30 %) doped TiO<sub>2</sub>.

Compositins	Ti (wt. %)	O (wt.%)	Zn (wt. %)
TiO <sub>2</sub>	73.90	26.10	0.00
1% Zn	71.09	27.40	1.51
5% Zn	69.96	24.23	5.80
10% Zn	65.39	23.10	11.51
12% Zn	60.43	25.70	11.51
30% Zn	51.16	20.12	28.72

D. Fourier Transform Infrared Spectroscopy (FTIR)

Absorption spectrum of the Zn doped samples was observed by spectrum 100, Perkin Elmer Instruments. The results are shown in Figure 7.

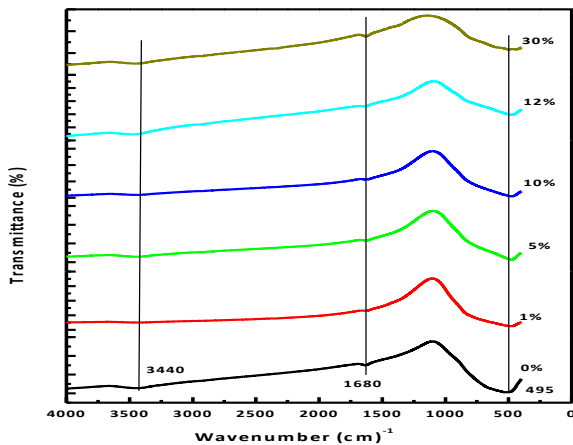


Fig. 7. FTIR spectra of Zn (0, 1, 5, 10, 12 and 30 %) doped TiO<sub>2</sub>

The broad absorptions around 3440 and 1680 cm<sup>-1</sup> are assigned to the hydroxyl groups of chemisorbed and physisorbed water molecules on the samples. A strong absorption band near 495 cm<sup>-1</sup> reveals the vibration properties of ZnO. Other unmarked peaks are attributed to organic species in the samples.

E. UV-Vis Diffuse Reflection Spectroscopy

In order to study the optical response of pure TiO<sub>2</sub> and Zn (0, 1, 5, 10, 12 and 30 %) doped TiO<sub>2</sub> samples, the UV-Vis spectra were measured as shown in the Tauc plot in Figure 8.

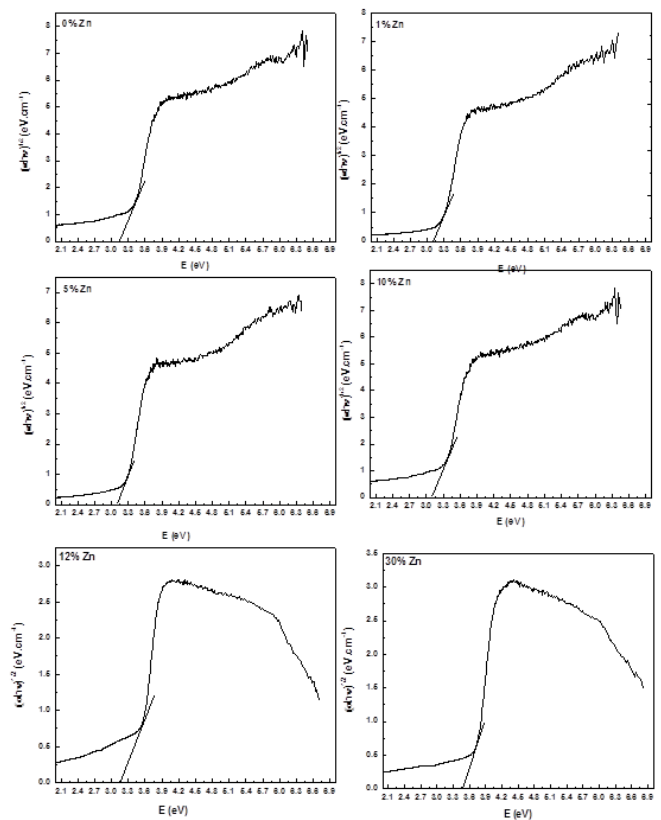


Fig. 8. Tauc plot of Zn (0, 1, 5, 10, 12 and 30 %) doped TiO<sub>2</sub> photocatalysts.

All the samples reveal an optical absorption below 400 nm which is attributed to electron Ti-O transition of nanocrystalline TiO<sub>2</sub>. The results show a small shift to the red region (3.12-3.09 eV) for the TiO<sub>2</sub>-ZnO samples in comparison to TiO<sub>2</sub> reference sample (3.25 eV) [35] and results are listed in Table IV.

Table IV. Band gap energy results

Compositions	Bandgap (eV)
0 % Zn	3.25
1% Zn	3.17
5% Zn	3.12
10% Zn	3.09
12% Zn	3.09
30% Zn	3.26

Incorporation of ZnO to TiO<sub>2</sub> only results in small variations in the energy band gap [36]. On increasing the percentage of Zn, the band gap decreases a little but remain in the UV-region, it means that ZnO is present in the samples but not detected in the XRD pattern, might be due to the high dispersion on the titania surface [37].

## IV. Photocatalytic Hydrogen Production

The photocatalytic H<sub>2</sub> evolution from doped ZnO into TiO<sub>2</sub> was compared with that of bare TiO<sub>2</sub> and P25 as benchmarks. Figure 9 shows the hydrogen production as a function of the irradiation time for bare TiO<sub>2</sub>, P25 and coupled TiO<sub>2</sub>-ZnO (1%, 5%, 10%, 12% and 30%) nanocomposites.

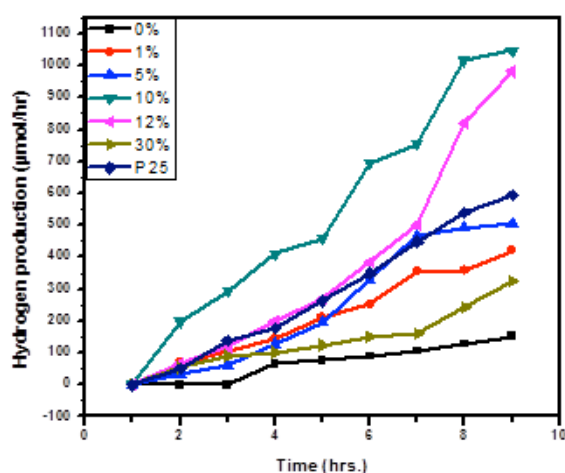


Fig. 9. H<sub>2</sub> evolution of bare TiO<sub>2</sub>, Degussa P25, 1% Zn, 5% Zn, 10% Zn, 12% Zn and 30% Zn samples.

It is clear that production of hydrogen increases with the increase of Zn contents. The mixed oxides give more active results better than bare TiO<sub>2</sub> already discussed by Larios et al [38]. Samples (0, 1, 5 and 10 %) have band gap of 3.24, 3.17, 3.12, and 3.09 eV respectively, so these phases can be excited by UV light. In these samples (0, 1, 5 and 10 %) the surface area increased systematically with increases of ZnO content 32.53, 52.08, 63.44, and 69.93 m<sup>2</sup>.g<sup>-1</sup> respectively. Generally, higher surface area material is beneficial for superior photocatalytic activity. On comparing these Samples (1, 5 and 10 % wt.% Zn) with Degussa P25, we observed P25 has product activity more than 1% Zn and 5% Zn but lower than that of 10% Zn content.

Despite the lower surface area of the commercial Degussa P25 (46 m<sup>2</sup>.g<sup>-1</sup>) than 1% Zn (52 m<sup>2</sup>.g<sup>-1</sup>) and 5% Zn (63 m<sup>2</sup>.g<sup>-1</sup>), this commercial product has a higher photoactivity in our specific testing conditions. This result tends to confirm that the morphology and interface of P25 anatase (80 wt.%) and rutile (20 wt.%) have an impact stronger than the surface area on the

H<sub>2</sub> photocatalytic generation. Since the obtained 10% Zn has activity higher than P25, it gives a clear indication that the amount of Zn has improved the evolution of hydrogen and got more activity than P25. On the basis of these results, it can be concluded that excited electrons from ZnO are trapped to conduction band of TiO<sub>2</sub> and produced electron-hole pair generation [38]. Hence, TiO<sub>2</sub>-ZnO composites with higher than 10 wt.% ZnO (12% and 30%) were found to be not favorable to obtain reasonable photocatalytic activity towards hydrogen generation as specific surface area was drastically decreased. Similar trends were observed after loading or mixing TiO<sub>2</sub> with ZnO or ZrO<sub>2</sub> [32-33]. Table V. sums up the features of the tested samples.

Table V. Textural properties, band gap energy (E<sub>g</sub>) and H<sub>2</sub> production for the TiO<sub>2</sub>-ZnO samples.

Sample	Phase	S <sub>BET</sub> (m <sup>2</sup> .g <sup>-1</sup> )	Pore diameter (nm)	P.V (cm <sup>3</sup> /g)	Band gap (eV)	H <sub>2</sub> production (µmol/hr)
TiO <sub>2</sub> (0%)	A	32.5	10.67	0.09	3.25	151
P25	A, R	46	30	0.09	3.24	595
1%	A	52	5.81	0.085	3.17	421
5%	A	63	5.19	0.093	3.12	505
10%	A	69	5.04	0.1	3.09	1047
12%	A	64	5.93	0.1	3.09	982
30%	A	36.6	6.19	0.062	3.25	324

## V. Conclusion

In this study, develop and characterization of Zn doped in TiO<sub>2</sub> photocatalyst nanocomposites with various compositions is carried out. These photocatalysts were investigated for photocatalytic H<sub>2</sub> generation from aqueous ethanol solution as electron donor under UV-light irradiation. In this setup, ethanol functions primarily as hole traps to prevent rapid electron-hole recombination. All TiO<sub>2</sub>-ZnO nanocomposites exhibited significant photocatalytic activities towards H<sub>2</sub> evolution. However, the relative hydrogen yield over TiO<sub>2</sub>-ZnO composites varies with the percent composition of ZnO to TiO<sub>2</sub>. The doped TiO<sub>2</sub>-ZnO photocatalysts with 10% Zn have shown enhanced H<sub>2</sub> production compared to individual TiO<sub>2</sub> and commercial Degussa P25. The hydrogen evolution and performance of photocatalyst increased with the moderate increase in Zn<sup>2+</sup> content, indicating that doping had a positive synergic effect on improving photocatalytic activity in TiO<sub>2</sub>-ZnO composites. With an appropriate Zn<sup>2+</sup> loading, the specific surface increased, consequently resulting in a large number of reaction sites on the composites leading to enhanced photocatalytic activity. Among the photocatalyst nanocomposites investigated, the 10 % ZnO photocatalyst exhibited higher H<sub>2</sub> generation over a time period of 9 h and its H<sub>2</sub> generation capability was found to be highest among

other photocatalyst materials. Our experimental results demonstrated that the excessive Zn<sup>+2</sup> above the optimal loading would result in a sharp decrease in specific surface and total pore volume consequently leading to reduction in photocatalytic activity.

### Acknowledgment

We cordially acknowledge King Abdulaziz City for Science and Technology (KACST) and Research Center of College of Engineering, King Saud University (KSU) for their financial support.

### References

- [1] L. Zajec, "Slow pyrolysis in a rotary kiln reactor: Optimization and experiment." Masters Thesis done at the School for Renewable Energy Science in affiliation with University of Iceland & the University of Akureyri, February 2011. Accessed from [http://skemman.is/stream/get/1946/7005/17751/1/Luka\\_Zajec.pdf](http://skemman.is/stream/get/1946/7005/17751/1/Luka_Zajec.pdf).
- [2] M. Balat, and E. Kirtay, "Major Technical Barriers to a "Hydrogen Economy"." *Energy Sources Part a-Recovery Utilization and Environmental Effects*. vol. 32 pp.863-876, March, 2010.
- [3] G. Marban, and T. Vales-Solis, "Towards the hydrogen economy?" *Int. J. of HydEnergy*, vol. 32, 1625-1637 August, 2007.
- [4] J. Zita, J. Krysa, U. Cernigoj, U. Stangar, J. Jirkovsky, and J. Rathousky, "Photocatalytic properties of different TiO<sub>2</sub> thin films of various porosity and titania loading". *Catal Today*, vol. 161, pp. 29-34, March, 2011.
- [5] M.L. Satuf, M.J. Pierrestegui, L. Rossini, R.J.Brandi, and O.M. Alfano, "Kinetic modeling of azo dyes photocatalytic degradation in aqueous TiO<sub>2</sub> suspensions." *Toxicity and biodegradability evaluation. Catal Today*, vol.161, pp. 121-126. March, 2011.
- [6] Y. H. Tseng, and C.H. Kuo, "Photocatalytic degradation of dye and NO<sub>x</sub> using visible-light-responsive carbon-containing TiO<sub>2</sub>." vol. 174, pp.114-120, October, 2011.
- [7] M. Uzunova-Bujnova, R. Kralchevska, M. Milanova, R. Todorovska, D.Hristova, and D.Todorovsky, "Crystal structure, morphology and photocatalytic activity of modified TiO<sub>2</sub> and of spray-deposited TiO<sub>2</sub> films." *Catal Today* vol. 151, pp.14-20, April, 2010.
- [8] S. Mozia, "Application of temperature modified titanate nanotubes for removal of an azo dye from water in a hybrid photocatalysis-MD process." *Catal Today* vol.156, pp.198-207, October, 2010.
- [9] C.A. Castro-López, A. Centeno, and S.A. Giraldo, "Fe-modified TiO<sub>2</sub> photocatalysts for the oxidative degradation of recalcitrant water contaminants." *Catal Today*, vol.157:119-124, November, 2010.
- [10] V. Rodríguez-González, M.A. Ruiz-Gómez, L. M. Torres-Martínez, R. Zanella, and R. Gómez, "Sol-gel silver hexatitanates as photocatalysts for the 4-chlorophenol decomposition." *Catal Today*, vol.148, pp.109-114. October, 2009
- [11] A.M.T. Silva, C.G. Silva, G. Drazic, and J.L. Faria, "Ce-doped TiO<sub>2</sub> for photocatalytic degradation of chlorophenol." *Catal Today*. vol.144, pp.13-18. June, 2009.
- [12] R. López, R. Gómez, and M.E. Llanos. "Photophysical and photocatalytic properties of nanosized copper-doped titania sol-gel catalysts." *Catal Today*, vol. 148, pp. 103-108, 2009.
- [13] C.L. Bianchi, G. Cappelletti, S. Ardizzone, S. Gialanella, A. Naldoni, and C. Oliva, "N-doped TiO<sub>2</sub> from TiCl<sub>3</sub> for photodegradation of air pollutants." *Catal Today*, vol. 144, pp.31-36, June, 2009.
- [14] A. Bernabeu, R.F. Vercher, L. Santos-Juanes, P.J. Simón, C. Lardín, and M.A. Martínez, "Solar photocatalysis as a tertiary treatment to remove emerging pollutants from wastewater treatment plant effluents." *Catal Today*, vol.161, 235-240. March, 2011.
- [15] P.S. Yap, T.T. Lim, and M. Srinivasan, "Solar photocatalysis as a tertiary treatment to remove emerging pollutants from wastewater treatment plant effluents." *Catal Today*, vol.161, 46. March, 2011.
- [16] I.H. Tseng, and J.C.S. Wu. "Chemical states of metal-loaded titania in the photoreduction of CO<sub>2</sub>." *Catal Today*. vol. 97:113-119, October, 2004.
- [17] T. Sreethawong, Y. Suzuki, and S. Yoshikawa."Photocatalytic evolution of hydrogen over mesoporous TiO<sub>2</sub> supported NiO photocatalyst prepared by single step sol-gel process with surfactant template." *Int J Hydrogen Energy* August, 2005.vol. 30:1053-1062
- [18] A. Erdölyi, J. Raskó, T. Kecskés, M. Tóth, M. Dömök, and K. Baán. "Hydrogen formation in ethanol reforming on supported noble metal catalysts." *Catal Today*. vol. 116:367-376. July, 2006.
- [19] L.S. Yoong, F.K. Chong, and B.K. Dutta. "Development of copper-doped TiO<sub>2</sub> photocatalysts for hydrogen production under visible light." *Energy* vol. 34, pp. 1652-1661, October, 2009.
- [20] D.V. Cêsar, R.F. Robertson, and N.S. Resende. "Characterization of ZnO and TiO<sub>2</sub> catalysts to hydrogen production using thermoprogrammed desorption of methanol." *Catal Today*, vol. 133-135, pp.136-141, June, 2008.
- [21] W.C. Lin, W.D. Yang, I.L. Haung, T.S. Wu, and Z.J. Chung, "Hydrogen production from methanol/water photocatalytic decomposition using Pt/TiO<sub>2</sub>-xNx catalyst." *Energy Fuel*, vol.23, pp.2192-2196, April, 2009.
- [22] F. Galindo-Hernández, and R. Gómez, "Degradation of the herbicide 2, 4- dichlorophenoxyacetic acid over TiO<sub>2</sub>-CeO<sub>2</sub> sol-gel photocatalysts: effect of the annealing temperature on the photoactivity." *Photochem Photobiol*, vol. 217, pp. 383-388, January 2011.
- [23] K.S Ahn, Y. Yan, S. Shet, K. Jones, T. Deutsch, J. Turner, and M. Al-Jassim, "ZnO nanocoral structures for photoelectrochemical cells." *Appl. Phys. Lett*, vol. 93, pp. 163117, October 2008.
- [24] P. Kajitvichyanukul, and T. Sungkaratana, "Photocatalytic Removal of Zinc (II) in UV -Irradiated Titania Suspensions" *As. J. Energy Env. Vol. 7*, pp. 258-265, 2006.
- [25] A. S. Huss, J. E. Rossini, D. J. Ceckanowicz, J. N. Bohnsack, K. R. Mann, W. L. Gladfelter, D. A. Blank, A. S. Bierbaum, A. Chitta, R. Ceckanowicz, D. J. Mann, K. R. Gladfelter, and W. L. Blank, "Photo-initiated Electron Transfer Dynamics of a Terthiophene Carboxylate on Monodispersed Zinc Oxide Nanocrystals." *J. Phys. Chem. C*, vol. 115, pp. 2-10, 2011.
- [26] M. Ni, M. K. H. Leung, D. Y. C. Leung, and K. Sumathy, "A review and recent developments in photocatalytic water-splitting using TiO<sub>2</sub> for hydrogen production." *Renewable Sustainable Energy Rev.* vol. 11 pp. 401-425, 2007.
- [27] T. K. Tseng, Y. S. Lin, Y. J. Chen, and H. Chu, "A Review of Photocatalysts Prepared by Sol-Gel Method for VOCs Removal." *Int. J. Mol. Sci.* vol.11 pp. 2336-2361, May 2010.
- [28] Y. Xu, and M.A. Schoonen, "The absolute energy positions of conduction and valence bands of selected semiconducting minerals." *Am Mineral.* vol. 85, pp. 543-56, 2000.
- [29] J.S. Jang, C.J. Yu, S.H. Choi, S.M. Ji, E.S. Kim, and J.S. LeeS. "Topotactic synthesis of mesoporous ZnS and ZnO nanoplates and their photocatalytic activity." *J Catal.* vol. 254, pp. 144-155, January 2008.
- [30] Highscore plus reference.
- [31] R.D. Shannon, "Revised effective ionic radii and systematic studies of interatomic distances in halides and chalcogenides." *Acta crystallographica*, vol. 32, pp. 751-767, September 1976.
- [32] Y. Wang, F. Li, W. Xue, and X. Zhao. "Clean synthesis of methyl N-phenyl carbamate over ZnO-TiO<sub>2</sub> catalyst." *J. Chem. Technol. Biotechnol*, vol. 84, pp. 48-53, January 2009.
- [33] B. Neppolian, Q. Wang, H. Yamashita, and H. Choi. "Synthesis and characterization of ZrO<sub>2</sub>-TiO<sub>2</sub> binary oxide semiconductor nanoparticles: application and inter- particle electron transfer process." *Appl. Catal*, vol. 333, pp. 264-271, December 2007.
- [34] A. Hussein, L. Mahoney, R. Peng, H. Kibombo, C. Wu, T. Ranjit, and R. Shende. "Mesoporous coupled ZnO/TiO<sub>2</sub> photocatalyst

- nanocomposites for hydrogen generation.” *Journal of Renewable and Sustainable Energy*, vol. 5, pp. 1-14, May 2013 .
- [35] Y. Xu, and M.A.A. Schoonen. “The absolute energy positions of conduction and valence bands of selected semiconducting minerals.” *Am Mineral*, vol. 85, pp 543-556, 2000.
- [36] A.L. Linsebigler, G. Lu, and J.T. Yates. “Photocatalysis on TiO<sub>2</sub> surfaces: principles, mechanisms and selected results.” *Chem Rev.* vol. 95, pp. 735-758, May 1995.
- [37] A. Mohamed, Q. Ahsanulhaq, H. Parameswar, and A.M. Wakas. “Formamide driven synthesis of well-aligned ZnO nanorod arrays on glass substrate.” *Mater Sci Semiconduct Proc.* vol. 13, pp. 113-118, June 2010.
- [38] P. Larios, R. Lopez, A. Hernandez-Gordillo, F. Tzompantzi , R. Gomez, and R. Torres-Guerra. “Improved hydrogen production from water splitting using TiO<sub>2</sub>-ZnO mixed oxides photocatalysts”. *Fuel*, vol. 100, pp.139-143, October 2012.